# High Strain Rate Characterization of Thermoplastic Fiber-Reinforced Composites under Compressive Loading

**Chapter** · May 2019

DOI: 10.5772/intechopen.82215

CITATION
1

READS
261

**9 authors**, including:

Carlos Vinicios Opelt
Centro Universitário - Católica de Santa Catarina
**18** PUBLICATIONS **293** CITATIONS
SEE PROFILE

Carolina Ramírez Montes
Autonomous University of Nuevo León
**4** PUBLICATIONS **4** CITATIONS
SEE PROFILE

Mauricio V. Donadon
Instituto Tecnologico de Aeronautica
**188** PUBLICATIONS **2,943** CITATIONS
SEE PROFILE

Vitor Reis
Instituto Tecnologico de Aeronautica
**11** PUBLICATIONS **106** CITATIONS
SEE PROFILE

Chapter

# High Strain Rate Characterization of Thermoplastic Fiber-Reinforced Composites under Compressive Loading

*Carolina Ramirez, Vitor Reis, Carlos Opelt, Rafael Santiago, Facundo Almeraya, Mauricio V. Donadon, Citlalli Gaona, Rene Croche and Miguel Angel Baltazar*

## Abstract

Experimental study on the mechanical behavior of polyphenylene sulfide (PPS)-based composite laminates reinforced with carbon and glass fibers subjected to different strain rates under compression load is reported. Quasi-static tests have been carried out using an electromechanical universal testing machine at three different strain rates, while dynamic tests were done using a split-Hopkinson pressure bar (SHPB) apparatus at two pressure setups in the gas chamber. High-speed imaging system was used to monitor failure process during dynamic test, and these images were used to measure strain by digital image correlation (DIC) in order to compare the DIC-based measurements performed with the SPHPB strain gauges and quasi-static results. Fractography analysis was also performed to identify the main failure mechanisms induced at different strain rates.

**Keywords:** high strain rate, split-Hopkinson pressure bar, thermoplastic fiber-reinforced composites, digital image correlation, fractography

## 1. Introduction

During service, aircraft structures are subjected to dynamic loads such as impact with foreign bodies, projectile impacts, and shock waves, which may significantly affect the mechanical properties of thermoplastic fiber-reinforced (TFR) composite materials used for these high-performance structures [1–3]. Thus, a reliable design of the composite components requires a detailed mechanical characterization at high strain rates because in most cases, due to the lack of dynamic properties, static properties are used in material selection and design, which can result in excessive structural weight or cause unexplained and untimely failure [1, 4–6].

Efforts have been made to determine the relation between fiber-reinforced polymer matrix composite (FRPC) mechanical properties at high strain rates and material configuration (resin and fiber length, concentration and orientation), using different high strain rate test techniques. Different authors have report and analyzed several researches as a state of the art in this topic; however, most of the studies are focused on thermoset composites, especially epoxy and polyester matrices reinforced with glass

and carbon fibers [3, 5, 7–13]. The few works found in open literature about thermoplastic composites studied polyamide-reinforced composites (with glass and carbon fiber with different fiber configurations), ethylene-propylene copolymer (EPC) matrix reinforced with discontinuous glass fibers, commingled e-glass/polypropylene woven fabric composite, glass fiber-reinforced polypropylene (PP) and polybutene-1 (PB-1), and AS4 graphite/polyetheretherketone (PEEK) thermoplastic composite [4, 11, 14–20]; however there is a lack of information about PPS matrix composite's behavior.

Among the several techniques to achieve high strain rates for tests [21], the split-Hopkinson pressure bar testing is often used for composite materials [3, 5, 10, 18, 22–29], where both the specimen stress-time and the specimen strain-time response are calculated from the strain waves measured on the bars. Additionally, high-speed camera technology with high resolution allow to apply optical and contactless strain field measurement techniques such as digital image correlation (DIC), to obtain accurate data reduction possibilities and more information on the distribution of strain over the specimen surface, which will be later employed in the dynamic material characterization [11, 26, 30, 31]. Within this context, the present work uses these techniques to characterize the strain rate effects on the mechanical behavior of PPS matrix carbon fiber-reinforced composite under compressive loadings in both static and dynamic regimes. Results obtained from dynamic statics are compared with quasi-static test results for the same specimen geometry and batch. Images obtained by high-speed imaging are used during tests to help to identify macro-failure modes induced at high strain rate tests, while micro-failure observation was carried out to identify quasi-static failure aspects and damage mechanisms of the material at all tested strain rates.

## 2. Methodology

### 2.1 Material

The materials used in this study are matrix polymeric (PPS, polyphenylene sulfide) fiber-reinforced composites, which were selected due to their application on aircraft structures such as leading edges, door structures, and pylon engine covers, among others [32–36]. These materials were provided by TenCate in the form of rectangular laminates in two versions:

a. 33-ply-thick laminate consisting of carbon fabric, 5HS style (harness-satin weave where one filling yarn floats over four warp yarns and under one, **Figure 1a**), 3K (3000 individual strands of carbon per fiber bundle) T300J (Toray Carbon Fibers America, Inc. specification, commonly used in aerospace applications), and 280 gsm FAW (fiber area weight in grams per square meter), combined with 42% RC (resin content by weight) Fortron 214 PPS in an orthotropic (0, 90) balanced/mirrored layup (**Figure 1a**)

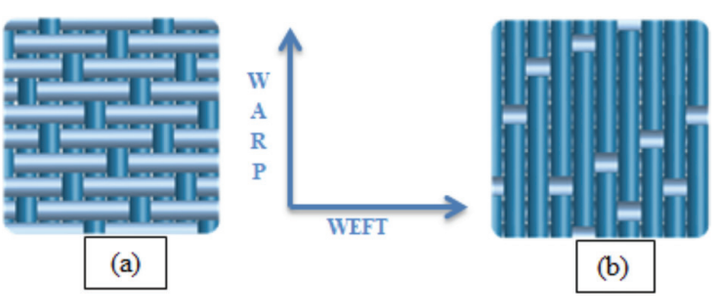


**Figure 1.**
*Harness-satin weave (a) 5HS and (b) 8HS [37].*

b. 42-ply-thick laminate consisting of fiberglass fabric, 8HS style (harness-satin weave where one filling yarn floats over seven warp yarns and under one, **Figure 1b**), EC6 yarn (e-glass continuous fiber with filament diameter of 6 μm), and 300 gsm FAW (fiber area weight in grams per square meter), combined with 33% RC (resin content by weight) Fortron 214 PPS in an orthotropic (0, 90) balanced/mirrored layup (**Figure 1b**).

Rectangular specimens of 9 × 10 × 9.8 $mm^3$ (width × length × height) were cut from the originals bars using the Extec Labcut 5000, available on the Lightweight Structures Laboratory of the Instituto de Pesquisas Tecnológicas (IPT), which guarantees samples with parallel tolerance of 0.03 mm. The geometry of the specimens was set between the ranges specified to accomplish with the assumptions made about inertia and friction effect [28]. **Figure 2** shows the specimen configuration; red arrows indicate the load direction.

## 2.2 Quasi-static test

Quasi-static reference tests were performed at the Lightweight Structures Laboratory (IPT), using an INSTRON servo-mechanic universal testing machine at three constant displacement rates (0.6, 6, and 60 mm/min), which corresponds to three quasi-static axial strain rates 0.001, 0.01, and 0.1 $s^{-1}$ by considering the nominal specimen length of 10 mm. Load measurements were recorded using universal testing machine hardware and software, while an Imetrum video gauge system synchronized with the testing machine was used to measure strain in the specimen. Using the software interface, target points were placed at the center of the specimen, and the strain measurements were recorded during the test; additional targets were set to monitor strain behavior.

Special testing fixtures, with load distribution system, were used in the testing machine movable head member in order to ensure alignment during specimen loading process. **Figure 3** represents a schematic setup for quasi-static tests.

Longitudinal compressive strength is calculated, for this regimen, according to expression $\sigma\_S = P/A_S$, where P is the applied load recorded by universal testing machine hardware and software and $A_S$ is the cross-sectional area of the specimen [38].

Strength and strain data are post-processed to build up the stress-strain curves for quasi-static regime and to calculate peak stress, strain at peak stress, and Young's modulus in order to compare mechanical properties with those obtained in the dynamic regime. Experimental Young's modulus is determined as the slope of the linear regression (LR) applied to the stress-strain curve in the range of strain data between 0.7 and 1%.

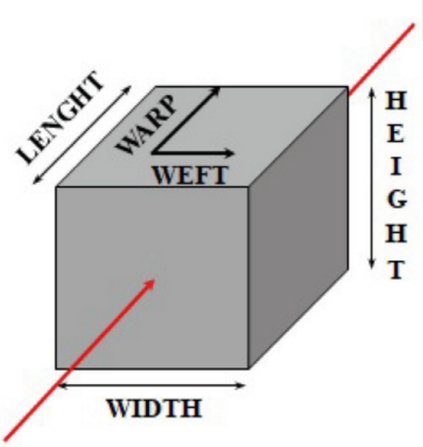


**Figure 2.**
*Isometric view of the specimen.*

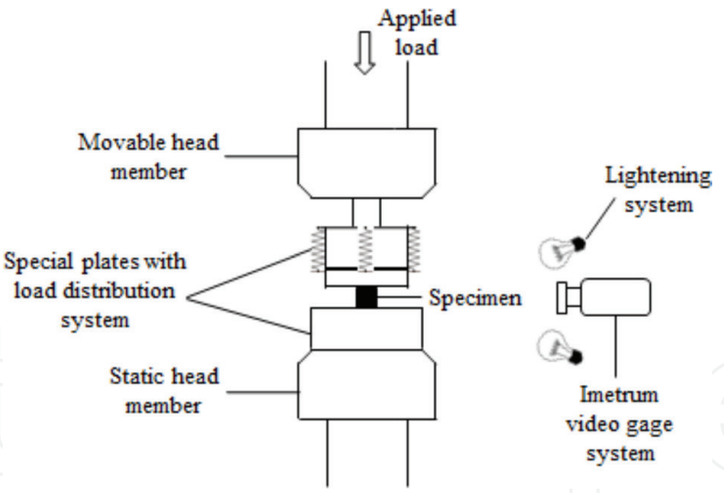


**Figure 3.**
*Quasi-static compression test setup.*

## 2.3 Dynamic test

High strain rate tests were performed using a split-Hopkinson pressure bar apparatus available in the Aerospace Structures Laboratory at Instituto Tecnológico de Aeronáutica (ITA) composed by three cylindrical bars: striker, incident, and transmitted bar. All three bars are made of high strength steel AMS 5629 with Young's modulus of 198 GPa, density of 7700 kg/m$^3$, yield stress of 1.4 GPa, and diameter of 19.05 mm. Striker length is 350 mm, and incident/transmission bars have 1000 mm, with length/diameter ratio of 50.0, that ensures the validity of unidimensional wave propagation assumption. The strain measurement system has four strain gauges HBM, model LY11–3/350 with 3 mm grid enabling measurements up to 100 kHz, which are disposed diametrically opposed in order to compensate bending and are located at 50 cm of the contact edge between specimen/incident bar and specimen/transmitted bar, respectively, and a data acquisition and conditioning system HBM Genesis 7 t, with a 16 bit resolution analog/digital card, four strain gauge channels, and sampling rate of 1 MHz. The present configuration has a momentum trap after the transmission bar to preserve the strain gauges [29, 39]. Additionally, a Photron high-speed imaging system (HSIS) composed of a high-speed camera model FASTCAM SA-Z and FASTCAM analysis software was set up with the SHPB apparatus to capture videos and images during the experiments. **Figure 4** shows the schematic SHPB testing setup used for the dynamic tests.

Data acquisition and conditioning system signals were post-processed using an in-house Python program, which computes the stress, strain, and strain rate on the specimen using the classical SHPB analysis based on the one-dimensional wave propagation theory, which implies elastic deformation in the bars during the tests, unidirectional elastic pulses propagate along the bars, uniform deformation process in the specimen, and no dispersion of waves throughout the bars and the specimen [11, 24, 26, 28, 29].

Tests were done at two different pressure values in the air chamber, 1.2 and 1.6 bar, which correspond to two different strain rates for each material (558.5 and 891.1 $s^{-1}$ for glass fiber, and 400.5 and 832.2 $s^{-1}$ for carbon fiber).

Stress-strain database were used to build up the stress–strain curves for specimens tested in dynamic regime and to calculate mechanical properties (peak stress, strain at peak stress, and Young's modulus). Experimental Young's modulus is determined as the slope of the linear regression (LR) applied to the stress-strain curve in the range of strain data between 0.7 and 1%.

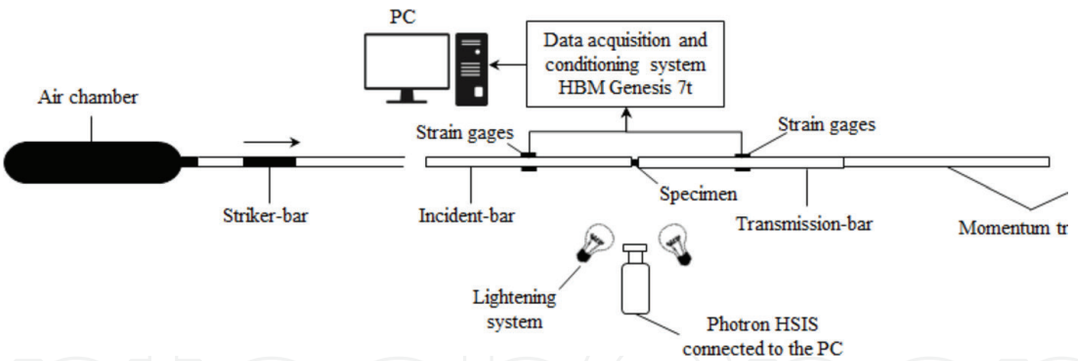


**Figure 4.**
*Schematic SHPB apparatus and HSIS set up.*


**Figure 5.**
*Inspect line Lo (middle white line) and overall area (purple square) used for DIC measurements.*

### 2.4 Digital image correlation

Digital image correlation (DIC) technique was used to measure strain during dynamic tests using the HSIS images obtained. 2D deformation vector fields and strain maps were built for specimens at each high strain rates tested, obtaining strain measures in an overall area and along an inspection line (L0) at each deformation state (**Figure 5**). Strain data from the center portion of the inspection line (L0) was synchronized with stress data from SHPB apparatus, and stress-strain curves were built using strain measured by DIC in order to compare the DIC-based results with the results obtained from SHPB strain gauge measurements and quasi-static regime results.

## 3. Experimental results and discussion

### 3.1 PPS carbon fiber-reinforced composite

#### *3.1.1 Quasi-static tests*

Quasi-static tests are performed to failure, under the three deformation rates previously specified (0.001, 0.01, and 0.1 $s^{-1}$). **Figure 6** shows stress-strain curves obtained for each strain rate applied, while **Table 1** summarizes the post-processed results. The results obtained show that material's peak stress remains constant under quasi-static regime with an average value of 532.603 MPa; this is based on the low value of the standard deviation (std. dev.) and the coefficient of variation (CV). The same

trend is observed for the Young's modulus obtaining an average value of 43.859 GPa. On the other hand, the strain at peak stress shows an average of 1.284% with a variation coefficient of 22.45%, which indicates that it varies considerably; however, it does not show a sensitivity on the strain rate or a correlation with a variation in the failure modes observed by fractographic observation, which indicates that dispersion in the measurements can be attributed to intrinsic errors in the measurement method. Having this in mind, it can be concluded that the mechanical behavior of the material is not strain rate sensitive within the strain rate range tested in the quasi-static regime.

*3.1.1.1 Fractographic observation*

Scanning electron microscopy (SEM) images for the specimens tested in the quasi-static regime can be observed in **Figure 7**. The material tested at 0.001 $s^{-1}$ (**Figure 7a**) presents a mixed failure mode (shear, yellow arrows; delamination, red arrows) due to the configuration of the fiber. Woven fiber laminates commonly present delamination through the warp fibers and shear through the weft fibers. Additionally, local kinkbands (**Figure 7a**, discontinued white lines) are evidenced in the warp fiber bundles, which is common in compression load failure due to the microbuckling that is developed in the fibers aligned in the direction of the load [40]. The specimens tested under 0.01 $s^{-1}$ (**Figure 7b**) and 0.1 $s^{-1}$ (**Figure 7c**) present similar behavior, which is observed a mixed failure mode (delamination and shear) and the development of local kinkbands. The material tested at 0.01 $s^{-1}$ develops intralaminar failure (discontinued yellow lines) related to the failure of the weft fibers and microbuckling (discontinued red line).

*3.1.2 Dynamic tests*

The dynamic tests are performed up to failure under two average strain rates of 400.5 and 832.3 $s^{-1}$; all these tests achieved equilibrium forces on specimen's surfaces, which is evidenced in **Figure 8** where forces applied on each contact surface of the specimen are showed for a test under each strain rate.

Stress-strain curves and data obtained for each strain rate applied at dynamic regime (**Figure 9** and **Table 2**) evidenced that the mechanical behavior of the material is not significantly affected by the strain rate effects presenting an average strength of 530.237 MPa, failure strain of 2.141%, and elasticity modulus of 34.273 GPa when strain is measured by SHPB strain gauges.

The same behavior remains when strain is measured by DIC; however the strain measured on the center portion of the specimen by DIC is lower than SHPB strain of about 38.856 and 36.605% for 400.5 and 832.3 $s^{-1}$, respectively, which leads to

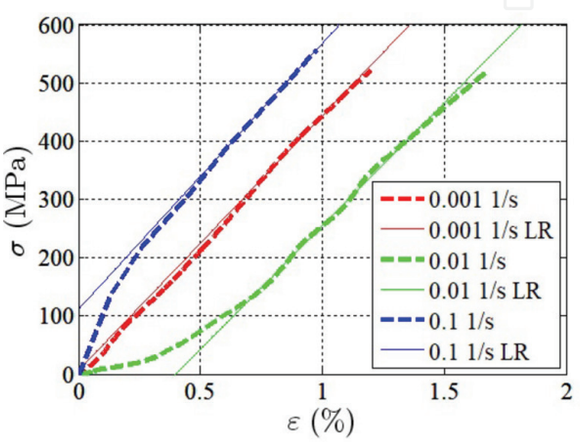


**Figure 6.**
*Stress-strain curve obtained for PPSCFC at quasi-static regime.*

| Strain rate ($s^{-1}$) | Peak Stress (MPa) | Strain at peak stress (%) | Young Modulus (GPa) |
|---|---|---|---|
| 0.001 | 521.926 | 1.203 | 43.664 |
| 0.01 | 517.869 | 1.67 | 42.271 |
| 0.1 | 558.013 | 0.978 | 45.643 |
| Average | 532.603 | 1.284 | 43.859 |
| Std. Dev. | 18.04 | 0.288 | 1.383 |
| CV (%) | 3.388 | 22.45 | 3.155 |

**Table 1.**
*Experimental results for PPSCFC at quasi-static regime.*

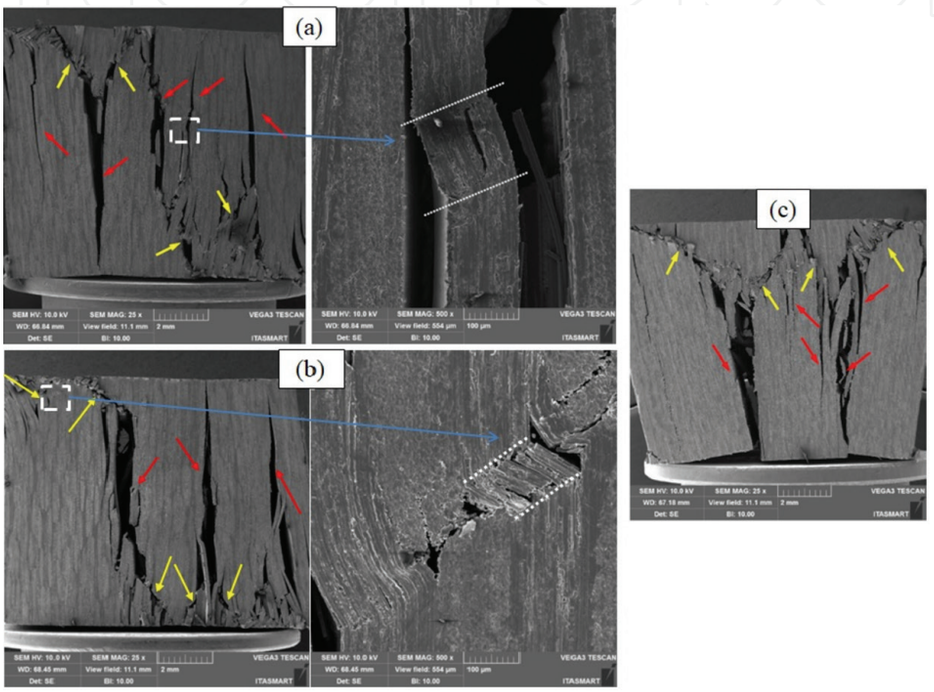


**Figure 7.**
*Quasi-static failure modes observation by SEM for PPSCFC under (a) 0.001 $s^{-1}$ (at 25× with amplified zone at 500×), (b) 0.01 $s^{-1}$ (at 25× with amplified zone at 500×) and (c) 0.1 $s^{-1}$.*

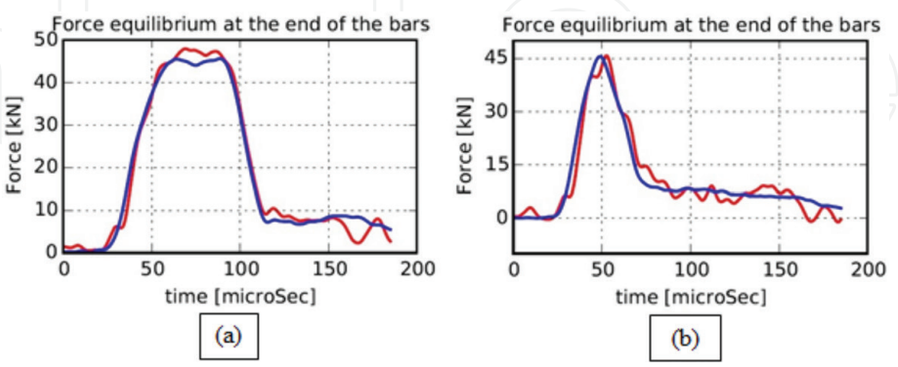


**Figure 8.**
*Force equilibrium on the edge of the incident bar (red line) and transmitted bar (blue line) for PPSCFC under (a) 400.5 $s^{-1}$ and (b) 832.3 $s^{-1}$.*

an increase in the Young's modulus of about 90.65% for 400.5 $s^{-1}$ and 71.606% for 832.3 $s^{-1}$. This difference can be seen in **Figure 10**, where stress–strain curves with strain measured by SHPB system and by DIC are shown at each tested strain rate.

The strain map for the overall area at the moment of the failure obtained by DIC strain analysis indicates that strain value measured by strain gauges was reached

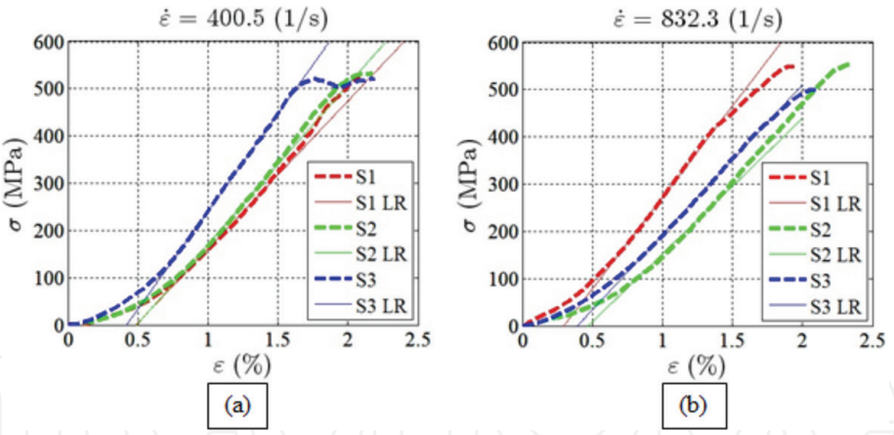


**Figure 9.**
*Stress-strain curves obtained under dynamic regime for PPSCFC. (a) 400.5 $s^{-1}$ and (b) 832.3 $s^{-1}$.*

| Strain rate ($s^{-1}$) | Peak Stress (MPa) | Strain at peak stress (%) | Young Modulus (GPa) |
|---|---|---|---|
| 400.5 | 525.747 | 2.148 | 35.493 |
| 832.3 | 534.726 | 2.134 | 33.053 |
| Average | 530.237 | 2.141 | 34.273 |
| Std. Dev. | 4.489 | 0.0073 | 1.22 |
| VC (%) | 0.847 | 0.341 | 3.559 |

**Table 2.**
*Comparison of mechanical properties under high strain rates for PPSCFC.*

in localized points of the specimen, generally on the edges (2.25% in the DIC spectrum and 2.088% according to SHPB measure for 400.5 $s^{-1}$; and 2437% on the DIC spectrum and 2.346% according to SHPB measure for 832.3 $s^{-1}$). This indicates that dynamic test behaves according to the theory and generates deformation highly localized or not homogeneous along the specimen due to the test high speed [24–26, 28, 41, 42]; also, the value measured by strain gauges is a real value of strain within the specimen; however, this value is the highest reached in all the specimen; in consequence, it is wise to measure strain by the DIC technique to obtain an accurate value on the center of the specimen where it can be assured that the behavior of the material is not influenced by the effect of the edges, where higher tendency to failure can be present as a consequence of the specimen machining [43].

*3.1.2.1 Fractographic observation*

The fractographic observation for dynamic regime is performed by monitoring the failure through the high-speed image system and SEM post-failure observation. **Figure 11** shows the sequence of the material's failure submitted to 400.5 $s^{-1}$ where the red arrow indicates the direction of the compressive wave. It can be observed the specimen at the beginning of the failure without any failure indication in **Figure 11a**; in the next image (**Figure 11b**) is shown the beginning of the failure on transmitted bar/specimen edge (blue circle), which is attributed to material's edges weakening by machining effect. The beginning of the failure is given in the form of delamination, and then it is propagated diagonally or in shear mode (**Figure 11c**). Besides, other two crack fronts are initiated on incident bar/specimen edge (blue circle **Figure 11c**), which join in a "v" shape, and then it is propagated in delamination mode. The specimen finishes its failure process with a partial separation of the surfaces (**Figure 11d**).

The material's failure process observed by HSIS for strain rate of 832.3 $s^{-1}$ is shown in **Figure 12**. The beginning of the failure is observed in two regions of the transmitted bar/specimen edge (blue circle) taking as reference the direction of wave propagation (red arrow) (**Figure 12b**). The upper region is submitted to bending, which is why the material looks bended upward, while the lower region develops two delamination fronts. The delaminations are propagated, while the bending on the upper region is intensified generating delamination and separation of the plies (**Figure 12c**) indicating failure of the resin, until the failure of the fibers under shear is initiated (**Figure 12d** yellow line). The propagation of the different crack fronts is prolonged until the specimen is entirely divided in several pieces (**Figure 12e**).

SEM fractographic observation was performed on the fracture surface of the different recovered parts of the material tested under 832.2 $s^{-1}$. **Figure 13a** shows a surface that appears to be "melted," while **Figure 13b–d** presents other surface that is "unmelted." This behavior indicates that heat generation during the test may have affected the crystallinity degree of the thermoplastic matrix. The "melted" surface (**Figure 13a**) is characterized for being smooth and without any distinctive features; observation at high zooms show the presence of fibrils in the interior of a crack, which look like resin threads that try to keep the crack faces together and oppose the propagation. On the "unmelted" surface (**Figure 13b**), two zones can be observed, Z1 which seems to be a zone directly over the fabric (it is not possible to identify if it is warp or weft) and Z2 which seems to be an interstitial site or a high resin content site. The zone Z1 (**Figure 13c**) shows cusps and scallops (red arrows),

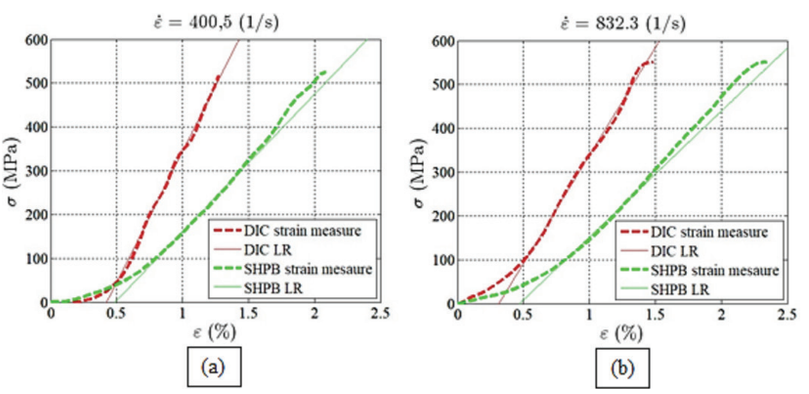


**Figure 10.**
*Stress-strain curve obtained for PPSCFC with strain measured by DIC and SHPB strain gages under (a) 400.5 $s^{-1}$ and (b) 832.3 $s^{-1}$.*

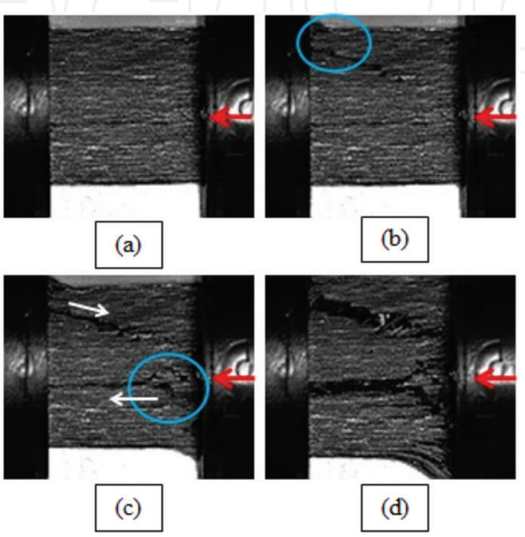


**Figure 11.**
*Images sequence taken by HSIS for PPSCFC tested at 400.5 $s^{-1}$.*

while the zone Z2 (**Figure 13d**) presents riverlines (yellow arrows) and feather marks (red circles). This fractographic aspects are typical of a composite submitted to compression [40, 44–46].

### *3.1.3 Mechanical property comparison for PPSCFC*

**Tables 3** and **4** present that the mechanical properties are not significantly affected by the strain rate effect while strain rate increases. Peak stress variation is less than 3.5% when results of specimens tested at quasi-static and dynamic regimes are compared, which indicate that strength is not strain rate dependent for this material. Strain at peak stress measured by the SHPB system presents higher variation than the strain measured by DIC (29.23–17.977%, respectively) compared with quasi-static results; however, the failure mechanism has not presented any difference which is why both can be considered negligible and the difference is attributed to the measurement method. The variation observed on the modulus is given by the obtained strain data; higher values for strain at peak stress obtained by SHPB gauges give modulus' lower values for dynamic tests and lower variation between quasi-static and dynamic regime compared with results with strain data measured by DIC; however, modulus is taking as constant, too, that is, it is not strain rate dependent.

Strain rate insensitivity is also observed in **Figure 14**, where peak stress-strain rate relation (a), strain at peak stress-strain rate relation (b), and Young's modulus-strain rate relation (c) are shown. Quasi-static (QS) and dynamic (D) average data is plotted for each property, differentiating SHPB strain data and DIC strain data.

It can be concluded that the material is not strain rate dependent and the measurement of dynamic strain by DIC allows a more accurate comparison with respect to the measurement of the quasi-static strain by the video strain gauge system. PPSCFC mechanical behavior discussed does not coincide with the behavior

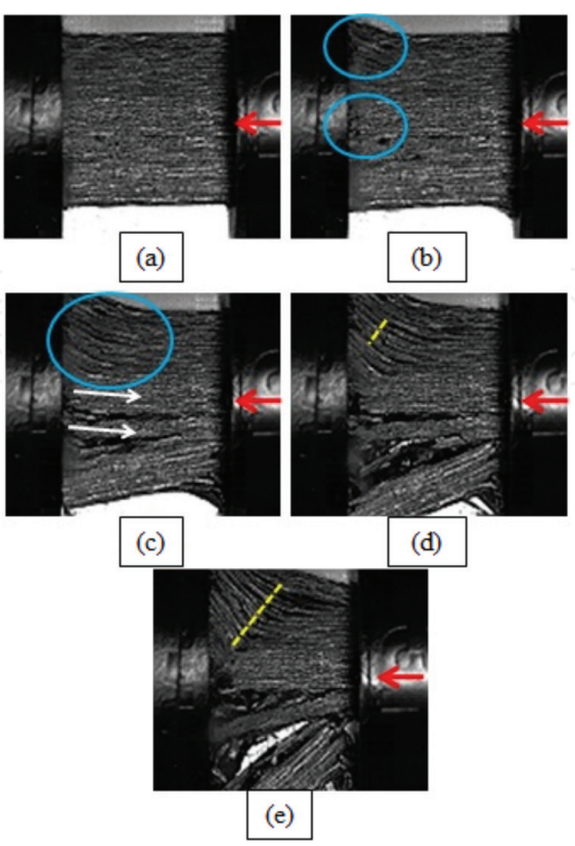


**Figure 12.**
*Images sequence taken by HSIS for PPSCFC tested at 832.2 $s^{-1}$.*

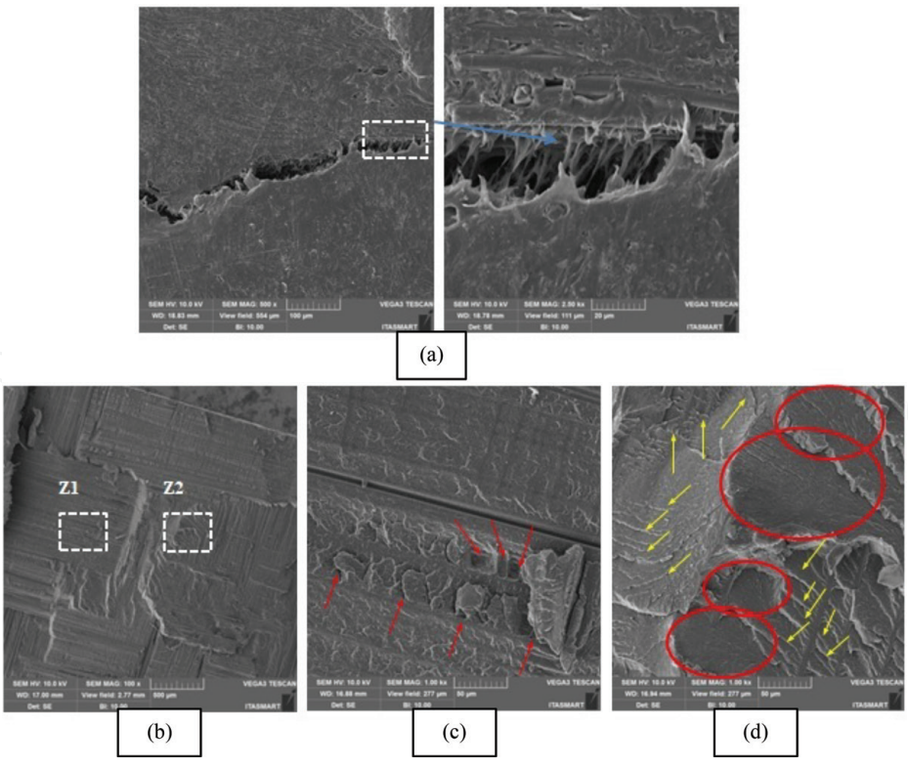


**Figure 13.**
*SEM images for PPSCFC tested at 832.3 $s^{-1}$. (a) "Melted" surface at 500× with 2500× zoom of the marked zone, (b) "unmelted" surface at 100×, (c) Z1 marked in (b) at 1000×, and (d) Z2 marked in (b) at 1000×.*

| Strain rate ($s^{-1}$) | Peak Stress (MPa) | Strain at peak stress (%) | Young Modulus (GPa) |
|---|---|---|---|
| 0.001 | 521.926 | 1.203 | 43.664 |
| 0.01 | 517.869 | 1.67 | 42.271 |
| 0.1 | 558.013 | 0.978 | 45.643 |
| 400.5 SHPB | 525.747 | 2.148 | 35.493 |
| 832.3 SHPB | 534.726 | 2.134 | 33.053 |
| Averga | 531.6564 | 1.6267 | 40.025 |
| Std.Dev. | 14.309 | 0.475 | 4.878 |
| CV (%) | 2.691 | 29.23 | 12.189 |

**Table 3.**
*Average mechanical properties for PPSCFC with strain measured by SHPB system.*

observed on similar materials (thermoplastic matrixes reinforced with carbon fiber) [11, 16, 19, 23, 27, 38]. This can be explained by the effect of carbon fiber on the resin (PPS) crystallization reported in open literature, where it has been found that transcrystallinity on the fiber-resin interphase affects the mechanical properties of the composite [32, 38, 47–49].

Failure mode is not strain rate dependent, either. The material presents mixed failure aspects (delamination and shear), which is characteristic for a laminate fabric submitted to compression according to Greenhalgh [40]. The material tested under the highest strain rate presents separation on multiple parts indicating severe damage due to the high-speed load application and insufficient dissipation of the heat generated in the deformation process. It is also worth to mention that it is observed that the delamination becomes more predominant at highest strain rate, which coincides with what Greenhalgh [40] reports for laminates submitted to high-speed impact loading.

| Strain rate ($s^{-1}$) | Peak Stress (MPa) | Strain at peak stress (%) | Young Modulus (GPa) |
|---|---|---|---|
| 0.001 | 521.926 | 1.203 | 43.664 |
| 0.01 | 517.869 | 1.67 | 42.271 |
| 0.1 | 558.013 | 0.978 | 45.643 |
| 400.5 DIC | 517.342 | 1.203 | 59.765 |
| 832.3 DIC | 552.518 | 1.487 | 49.263 |
| Average | 533.534 | 1.323 | 48.121 |
| Std. Dev. | 17.899 | 0.238 | 6.279 |
| CV (%) | 3.355 | 17.977 | 13.0479 |

**Table 4.**
*Average mechanical properties for PPSCFC with strain measured by DIC.*

### 3.2 PPS glass fiber-reinforced composite

#### *3.2.1 Quasi-static tests*

Quasi-static tests are performed to failure, under the three deformation rates specified (0.001, 0.01, and 0.1 $s^{-1}$). **Figure 15** shows stress-strain curves obtained for each strain rate applied, while **Table 5** summarizes the post-processed results. Sample S1 for 0.001 $s^{-1}$ tests was discarded due to reload during the test. The average value obtained for the peak stress for the quasi-static regime is 358.295 MPa with a coefficient of variation (CV) of 5.235%, which means that it is constant. Strain at peak stress and modulus presents the same behavior with values as of 1.676%–(CV) 8.875% and 21.999 GPa–(CV) 2.623%, respectively. Due to this it is said that mechanical behavior remains constant in quasi-static regime.

##### *3.2.1.1 Fractographic observation*

Fractographic observation by SEM for the PPSGFC specimens tested under quasi-static regime evidences a mixed failure mode (delamination and shear) for the laminate submitted to compression according to what is reported by Greenhalgh for fabrics [40]. **Figure 16** shows the failure modes for the three strain rates identifying delamination with red arrows and the shear with yellow arrows. The material tested at 0.001 $s^{-1}$ developed an early stage kinkband (**Figure 16b**), which indicates basic failure mode for composites under compression [38, 40, 44]. **Figure 16e** indicates the formation of a fiber bridging characteristic of mode I delamination (opening) [44].

#### *3.2.2 Dynamic tests*

The dynamic tests are performed up to failure under two average strain rates of 558.5 and 891.1 $s^{-1}$; all these tests achieved equilibrium forces on specimen's surfaces which is evidenced in **Figure 17** where forces applied on each contact surface of the specimen are showed for a test under each strain rate.

According to the results (**Figure 18** and **Table 6**), material's mechanical behavior is constant for the dynamic regime presenting 491.554 MPa as peak stress, 2.647% as failure strain, and 22.498 GPa as Young's modulus when strain is measured by SHPB strain gauges.

For this material it is also performed the strain measurement processing the high-speed videos under DIC, as it was done for the PPSCFC. **Figure 19** shows

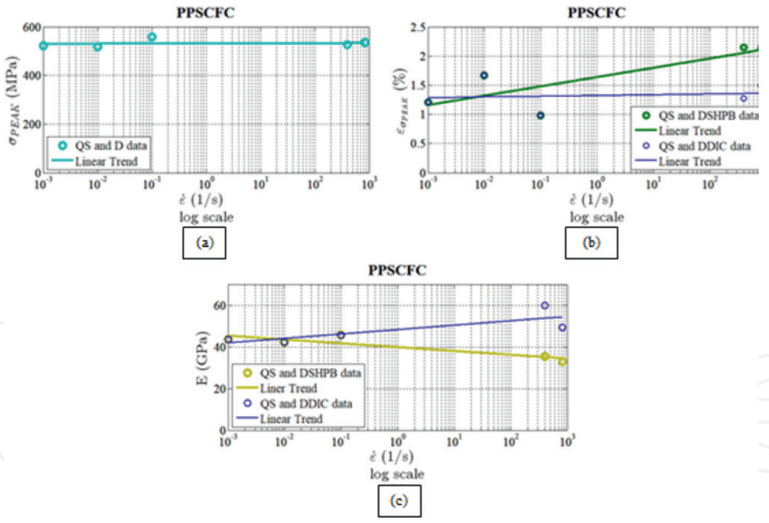


**Figure 14.**
*PPSCFC properties as function of the strain rate: (a) strength-strain rate plot, (b) ultimate strain-strain rate plot and (c) Young's modulus-strain rate plot.*

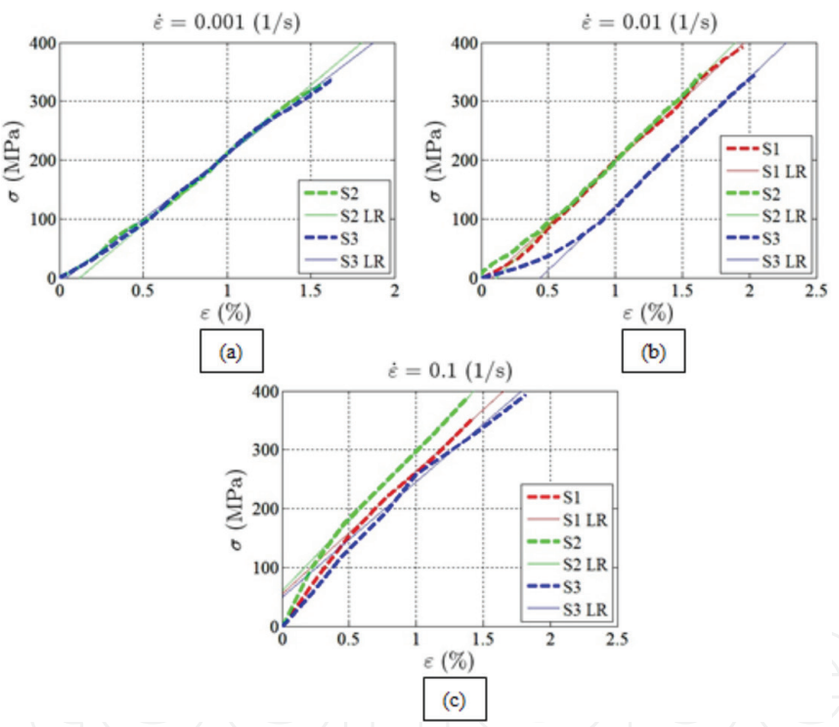


**Figure 15.**
*Stress-strain curve obtained for PPSGFC under compression at (a) 0.001 $s^{-1}$, (b) 0.01 $s^{-1}$ and (c) 0.1 $s^{-1}$.*

| Strain rate ($s^{-1}$) | Peak Stress (MPa) | Strain at peak stress (%) | Young Modulus (GPa) |
|---|---|---|---|
| 0.001 | 333.421 | 1.606 | 22.786 |
| 0.01 | 362.757 | 1.883 | 21.79 |
| 0.1 | 378.708 | 1,539 | 21.419 |
| Average | 358.295 | 1.676 | 21.999 |
| Std. Dev. | 18.756 | 0.149 | 0.577 |
| CV (%) | 5.235 | 8.875 | 2.623 |

**Table 5.**
*Experimental results for PPSGFC at quasi-static regime.*

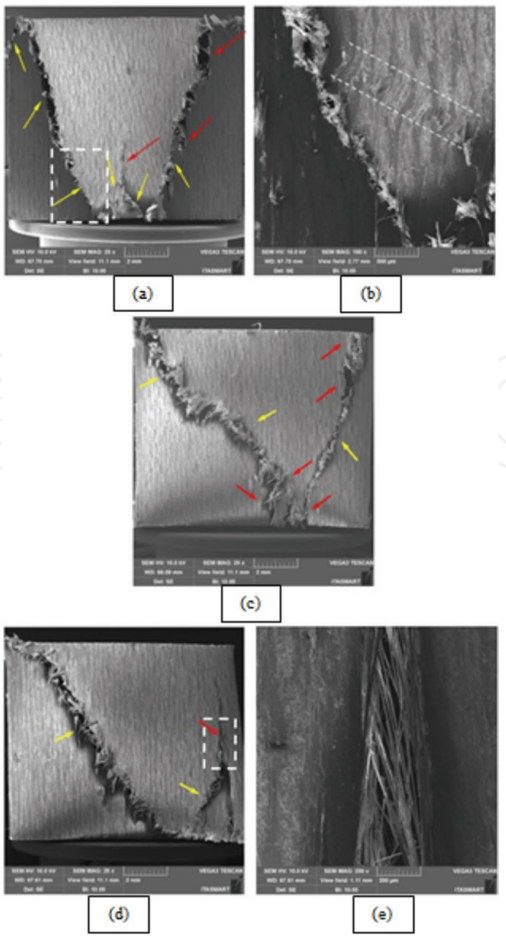


**Figure 16.**
*SEM images for PPSGFC tested under quasi-static strain rates. (a) 0.001 $s^{-1}$ at 25×, (b) marked zone in (a) at 100×, (c) 0.01 $s^{-1}$ at 25×, (d) 0.1 $s^{-1}$ at 25× and (e) marked zone in (d) at 250×.*

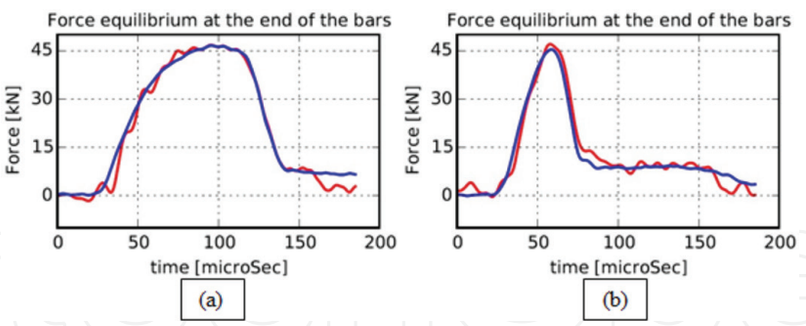


**Figure 17.**
*Force equilibrium on the edge of the incident bar (red line) and transmitted bar (blue line) for PPSGFC under (a) 558.5 $s^{-1}$ and (b) 891.1 $s^{-1}$.*

the variation of the stress-strain curves built up with the strain data measured by SHPB and DIC. Results obtained for this material are similar to PPSCFC; the strain measured by DIC is lower in 25.495 and 19.627% for 558.5 and 891.1 $s^{-1}$, respectively, with respect to the deformation measured with the SHPB strain gauges. As it was expected, the peak stress remains equal what leads to modulus increase (38.054% for 558.5 $s^{-1}$ and 6.553% for 891.1 $s^{-1}$) with respect to the data obtained by the SHPB.

The behavior observed in the strain map obtained by DIC is the same to the one analyzed for PPSCFC; the highest strain is very close to the value measured by the SHPB system (2.437% DIC–2.573% SHPB at 558.5 $s^{-1}$; 2.843% DIC–2.68% SHPB at 891.1 $s^{-1}$), which reaffirms what was previously said; the SHPB system obtains the highest strain value in the entire specimen. Resulting strain in the specimen is not

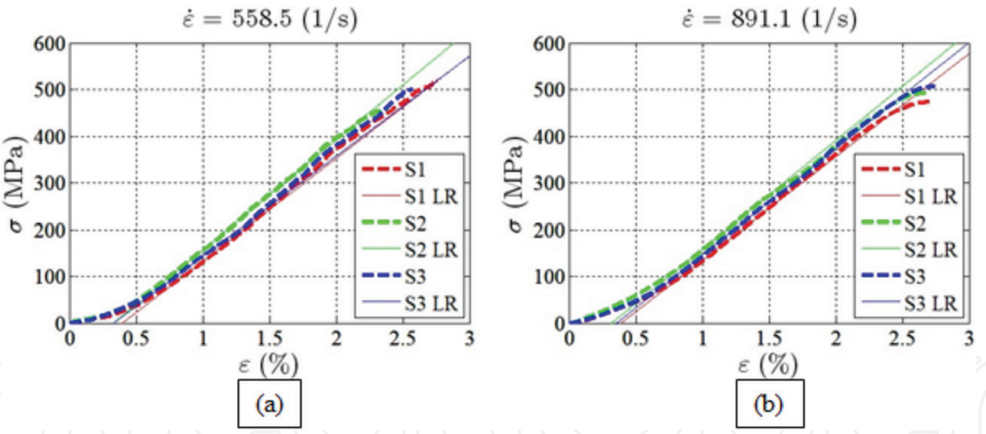


**Figure 18.**
*Stress-strain curves obtained under dynamic regime for PPSGFC: (a) 558.5 $s^{-1}$ and (b) 891.1 $s^{-1}$.*

| Strain rate ($s^{-1}$) | Peak Stress (MPa) | Strain at peak stress (%) | Young Modulus (GPa) |
|---|---|---|---|
| 558.5 | 491.886 | 2.575 | 22.293 |
| 891.1 | 491.223 | 2.719 | 22.703 |
| Average | 491.554 | 2.647 | 22.498 |
| Std.Dev. | 0.332 | 0.072 | 0.205 |
| CV (%) | 0.067 | 2.7322 | 0.912 |

**Table 6.**
*Comparison of mechanical properties under high strain rates for PPSGFC.*

homogeneous along it and is more critical on the edges, and the measurement of the strain DIC allows obtaining data without the influence of the machining.

*3.2.2.1 Fractographic observation*

The same that for PPSCFC, failure process monitoring is performed for PPSGFC through the high-speed image system; additional SEM post-failure observation was realized.

Images for material tested at 558.5 $s^{-1}$ (**Figure 20**) indicate that the failure starts on the specimen/transmitted bar contact edge and it propagates as delamination (**Figure 20b** and **c**, white arrow). A second crack front is developed on the inferior part of the specimen/incident bar contact edge in shear (**Figure 20c**, blue circle), which propagates and meets other crack front forming a "v" shape and continuing the propagation as delamination (**Figure 20d**), resulting in a mixed failure mode (delamination and shear).

Failure behavior for the material tested at 891.1 $s^{-1}$ is similar to that observed in specimens tested in other strain rates. The beginning of the failure starts on the inferior region of the specimen/transmitted bar contact edge, and it propagates in shear (**Figure 21b**, blue circle); on its way it is bifurcated; and on one side, it continues in shear toward the superior opposite edge; and on the other side, it propagates as delamination forming a "v" shape in the material (**Figure 21c**, white arrows). Additionally, another crack front is developed on the superior part of the specimen/transmitted bar contact edge in form of delamination, which is propagated separating the part and allowing relative movement with respect to the other parts (**Figure 21d**). For this strain rate, the material is divided in several parts which were submitted to SEM observation on the fracture surface.

The analysis of the fracture surface for the material tested at 891.1 $s^{-1}$ indicates the development of two types of surface as in the PPSCFC on the highest strain rate. A surface appears "melted" (**Figure 22a**), while the other appears "unmelted" (**Figure 22b**). The "melted" surface exhibits signs of abrasive wearing possibly due to the movement between sheets observed on the HSIS images [50, 51], while the "unmelted" surface presents cusps (red circle) which appears to be the weft as in mode I (opening) [44].

### *3.2.3 Mechanical property comparison for PPSGFC*

The data obtained by the SHPB system (**Table 7**) evidence an increase of 27% on the peak stress when the average values for the quasi-static and dynamic regimes are compared (358.295 and 491.554 MPa). Similarly, the deformation on the ultimate stress is increased by 36% when the average values for the quasi-static and dynamic regimes are compared (1.676 and 2.647%). It was not evidenced a significant change in the Young's modulus for the material tested in the dynamic regime with respect to that of the semi-static regime (2% increase).

According to the data obtained when strain is measured by DIC (**Table 8**), the tendency of strength increase is kept at 38% when the averages of the quasi-static

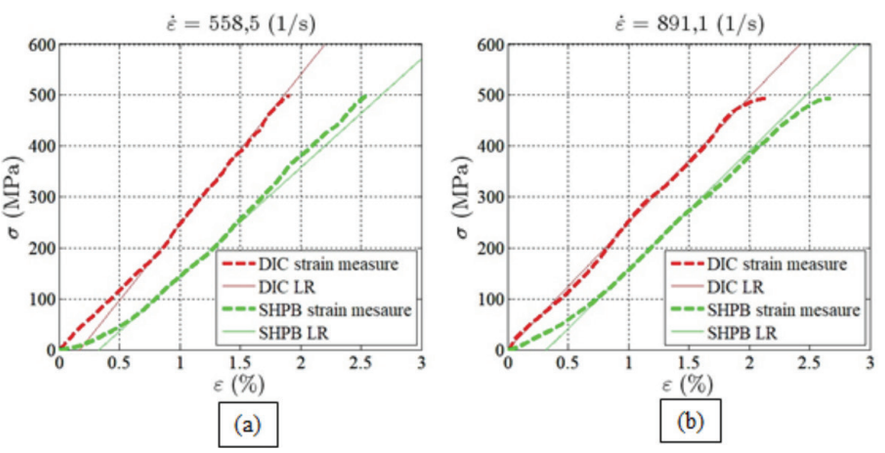


**Figure 19.**
*Stress-strain curve obtained for PPSGFC with strain measured by DIC and SHPB strain gages under (a) 558.5 $s^{-1}$ and (b) 891.1 $s^{-1}$.*

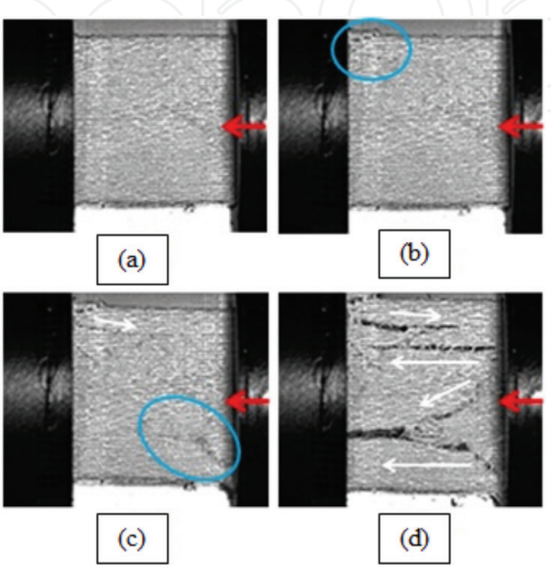


**Figure 20.**
*Images sequence taken by HSIS for PPSGFC tested at 558.5 $s^{-1}$.*

and dynamic regimes are compared (358.295 and 496.758 MPa), which is expected given that the determination of the peak stress is made with the same data. However, the increase in the strain at peak stress is just 21% based on the average values for each regime (1.676% quasi-static and 2.034% dynamic). The aforementioned affects the behavior of the Young's modulus, which presents an increase of 23% according to the average values for quasi-static and dynamic regimes (21.999 and 27.168 GPa). The behavior previously described is graphically evidenced in **Figure 23** where the properties' tendency with respect to the strain rate is shown.

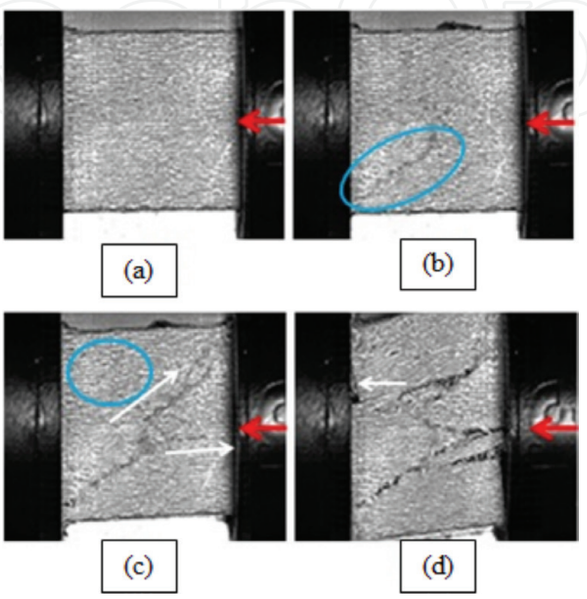


**Figure 21.**
*Images sequence taken by HSIS for PPSGFC tested at 891.1 $s^{-1}$.*

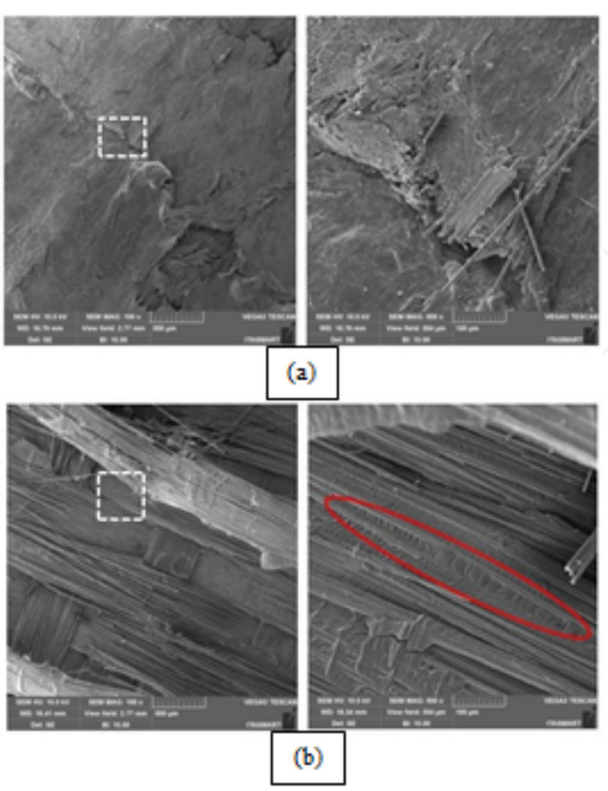


**Figure 22.**
*SEM images for PPSGFC tested at 891.1 $s^{-1}$. (a) "Melted" surface at 100× with 500× zoom of the marked zone, (b) "un-melted" surface at 100× with 500× zoom of the marked zone.*

| Strain rate ($s^{-1}$) | Peak Stress (MPa) | Strain at peak stress (%) | Young Modulus (GPa) |
|---|---|---|---|
| 0.001 | 333.421 | 1.606 | 22.786 |
| 0.01 | 362.757 | 1.883 | 21.79 |
| 0.1 | 378.708 | 1.539 | 21.419 |
| 558.5 SHPB | 491.886 | 2.575 | 22.293 |
| 891.1 SHPB | 491.223 | 2.719 | 22.703 |
| Average | 411.599 | 2.065 | 22.198 |
| Std. Dev. | 66.881 | 0.492 | 0.526 |
| CV (%) | 16.249 | 23.822 | 2.369 |

**Table 7.**
*Average mechanical properties for PPSGFC with strain measured by SHPB system.*

| Strain rate ($s^{-1}$) | Peak Stress (MPa) | Strain at peak stress (%) | Young Modulus (GPa) |
|---|---|---|---|
| 0.001 | 333.421 | 1.606 | 22.786 |
| 0.01 | 362.757 | 1.883 | 21.79 |
| 0.1 | 378.708 | 1.539 | 21.419 |
| 558.5 DIC | 494 | 2.154 | 24.781 |
| 891.1 DIC | 499.517 | 1.914 | 29.556 |
| Average | 413.681 | 1.819 | 24.067 |
| Std. Dev. | 69.393 | 0.223 | 2.982 |
| CV (%) | 16.774 | 12.275 | 12.392 |

**Table 8.**
*Average mechanical properties for PPSGFC with strain measured by DIC.*

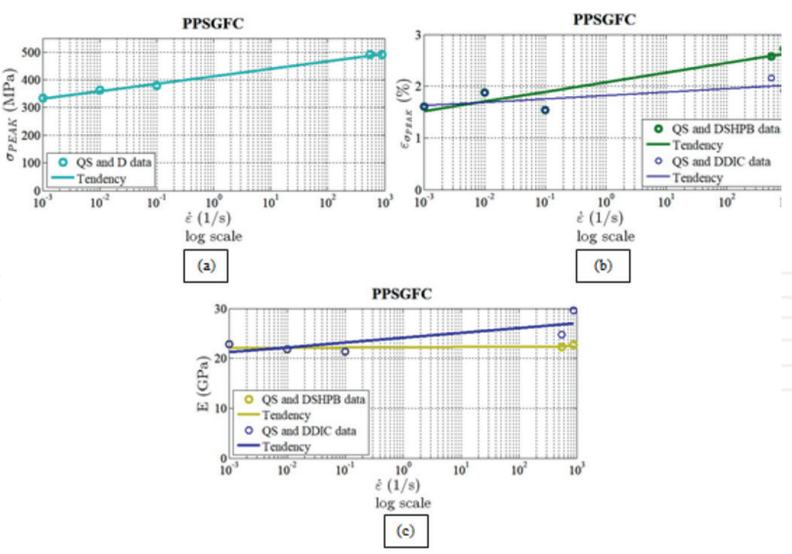


**Figure 23.**
*PPSCFC properties as function of the strain rate: (a) strength-strain rate plot, (b) ultimate strain-strain rate plot and (c) Young's modulus-strain rate plot.*

Results indicate that the material is strain rate dependent presenting an increase in the properties when strain rate applied increases, which is evidenced more accurately with DIC strain measurement and comparing it with the quasi-static results. The mechanical behavior observed on this material coincides with data reported for other similar materials in open literature (thermoplastic matrixes reinforced with glass fibers) [4, 16–18, 38, 52, 53].

The fractographic observation performed in both regimes indicates that the failure mechanism is not strain rate dependent since there is no significant variation in the failure aspects observed in specimens tested at high strain rates in comparison to those tested quasi-statically. The failure mechanism for the material is mixed (delamination and shear) in all the strain rates with a notorious dominance of the shear mode, which in the high deformation rates becomes balanced with the delamination. This behavior is expected due to the tendency of the glass fiber to fail at 45° when submitted to compression, and the laminate dilation turns the material more susceptible to delamination at high strain rates, according to Greenhalgh [40].

## 4. Conclusions

The mechanical behavior of the materials is linear elastic at all tested strain rates. Mechanical properties remain constant with respect to the strain rate applied for each regime. Results obtained for PPSCFC indicate compressive strength of 532.603 MPa, failure strain of 1.284%, and Young's modulus of 43.859 GPa for quasi-static regime and 534.93 MPa for compressive strength, 1.345% for failure strain, and 53.014 GPa for Young's modulus at high strain rates. PPSGFC results give compressive strength of 358.295 MPa, failure strain of 1.676%, and Young's modulus of 21.999 GPa for quasi-static regime and for the dynamic regime 496.758 MPa for compressive strength, 2.034% for strain failure, and 27.168 GPa for Young's modulus.

Comparing the obtained values for the mechanical properties calculated under the quasi-static and dynamic regimes, it is found that the PPSCFC exhibits a strain rate insensitive mechanical behavior with respect to the strain rates applied, while the PPSGFC is strain rate dependent, which means enhancement on mechanical properties when the strain rate increased. Compressive strength increases by 38%, failure strain increases by 21%, and Young's modulus increases by 23%.

According to the strain spectrum obtained from the strain measurement by DIC, the strain measurement by the SHPB system shows the highest strain value in the specimen; however, due to the strain behavior at dynamic tests, it is better to perform strain localized measurement, in order to compare mechanical properties calculated in both regimes.

The behavior for the PPSCFC reported herein is not in accordance with data and similar material reports elsewhere. This can be attributed to the fact that the resin used for this material (PPS) is semicrystalline and presents a reaction with the carbon fibers at the crystallization moment during the cooling, generating transcrystallinity on the fiber-resin interphase which affects the mechanical properties. Further studies must be performed to establish if this is why the material behavior is affected.

The behavior obtained for the PPSGFC is what is expected according to data and similar material reports published in the literature; the strain rate dependency of the mechanical properties is attributed to the viscoelasticity of the resin.

The failure mode observed for the materials, in general terms, is mixed. Delamination and shear mode are identified, and it is observed that the failure aspects are not significantly affected by strain rates, which in tum leads to conclude that the failure mechanism is not strain rate dependent. The failure mechanisms are governed by the material configuration and the fiber-resin interphase more than the strain rate applied, which explain that typical fractographic characteristics for composite materials submitted to uniaxial compression were developed.

Bigger efforts must be made to understand the generation and dissipation of heat during the material strain process for high strain rates to understand better their effect on the fractographic aspects of the material ("melted" surfaces).

## Acknowledgements

We also thank the Academic Body UANL-CA-316 "Deterioration and integrity of composite materials," the Conacyt for the scholarship for graduate studies, and the partial support by the CNPq processes 301053/2016-2, FINEP 0114018300.



## Author details

Carolina Ramirez[1], Vitor Reis[2,3], Carlos Opelt[3], Rafael Santiago[4], Facundo Almeraya[1], Mauricio V. Donadon[3], Citlalli Gaona[1*], Rene Croche[5] and Miguel Angel Baltazar[6]

1 Facultad de Ingeniería Mecánica y Eléctrica, Centro de Investigación e Innovación en Ingeniería Aeronáutica, Universidad Autónoma de Nuevo León, San Nicolás de los Garza, Nuevo León, México

2 Lightweight Structures Laboratory, Instituto de Pesquisas Tecnológicas – IPT, Technology Park of São Jose Dos Campos, São Paulo, Brazil

3 Laboratório de Estruturas Aeroespaciais, Instituto Tecnológico de Aeronáutica – ITA, São Jose Dos Campos, São Paulo, Brazil

4 Centro de Engenharia, Modelagem e Ciências Sociais Aplicadas – CECS, Universidade Federal do ABC, São Bernardo do Campo, São Paulo, Brazil

5 Facultad de Ingeniería Mecánica y Eléctrica - Xalapa, Universidad Veracruzana, Xalapa, Veracruz

6 Facultad de Ingeniería Civil - Xalapa, Universidad Veracruzana, Xalapa, Veracruz

*Address all correspondence to: citlalli.gaona@gmail.com

## References

[1] Hosur MV, Alexander J, Vaidya UK, Jeelani S, Mayer A. High strain rate compression characterization of affordable woven carbon/epoxy composites under off-axis loading. Polymers and Polymer Composites. 2003;**11**(7):527-539

[2] Federal Aviation Administration. Pilot's Handbook of Aeronautical Knowledge. Oklahoma: United State Department of Transportation; 2016

[3] Hosur MV, Alexander J, Jeelani S, Vaidya UK, Mayer A. High strain compression responses of affordable woven carbon/epoxy composites. Journal of Reinforced Plastics and Composites. 2003;**22**(3):271-296

[4] Fitoussi J, Bocquet M, Meraghni F. Effect of the matrix behavior on the damage of ethylene-propylene glass fiber reinforced composite subjected to high strain rate tension. Composites Part B: Engineering. 2012;**45**:1181-1191

[5] Hamouda AMS, Hashmi MSJ. Testing of composite materials at high rates of strain: Advances and challenges. Journal of Materials Processing Technology. 1998;**77**:327-336

[6] Jadhav A. High Strain Rate Properties of Polymer Matrix Composites. Luisiana, EU: Louisiana State University and Agricultural and Mechanical College; 2003

[7] Cantwell WJ, Morton J. The impact resistance of composite materials—A review. Composites. 1991;**22**(5):347-362

[8] Barré S, Chotard T, Benzeggagh ML. Comparative study of strain rate effects on mechanical properties of glass fibre-reinforced thermoset matrix composite. Composites Part A: Applied Science and Manufacturing. 1996;**27**:1169-1181

[9] Jacob GC, Starbuck JM, Fellers JF, Simunovic S, Boeman RG. Strain rate effects on the mechanical properties of polymer composite materials. Journal of Applied Polymer Science. 2004;**94**:296-301

[10] Dash K, Sukumaran S, Ray BC. Effect of loading speed on deformation of composite materials: A critical review. Journal of Advanced Research in Manufacturing, Material Science & Metallurgical Engineering. 2014;**1**:1-22

[11] Ploeckl M, Kuhn P, Koerber H. Characterization of unidirectional carbon fiber reinforced polyamide-6 thermoplastic composite under longitudinal compression loading at high strain rate. EPJ Web of Conferences. 2015;**94**(01041):1-6

[12] Koerber H, Camanho PP. High strain rate characterisation of unidirectional carbon-epoxy IM7-8552 in longitudinal compression. Composites Part A: Applied Science and Manufacturing. 2011;**42**:462-470

[13] Song Z, Wang Z, Ma H, Xuan H. Mechanical behavior and failure mode of woven carbon/epoxy laminate composites under dynamic compressive loading. Composites. Part B, Engineering. 2014;**60**:531-536

[14] Montiel DM, Williams CJ. Method for Evaluating the High Strain-Rate Compressive Properties of Thick Composite Laminates. Research and Development Report, DTRC-SME-90/28. Bethesda, USA: David Taylor Research Center; August 1990

[15] Weeks CA, Sun CT. Modeling non-linear rate-dependent behavior in fiber-reinforced composites. Composites Science and Technology. 1998;**58**:603-611

[16] Todo M, Takahashi K, Béguelin P, Kausch HH. Strain-rate dependence of

the tensile fracture behaviour of woven-cloth reinforced polyamide composites. Composites Science and Technology. 2000;**60**:763-771

[17] SchoBig M, Bierögel C, Grellmann W, Mecklenburg T. Mechanical behavior of glass-fiber reinforced thermoplastic materials under high strain rates. Polymer Testing. 2008;**27**:893-900

[18] Brown KA, Brooks R, Warrior NA. The static and high strain rate behaviour of a commingled E-glass/polypropylene woven fabric composite. Composites Science and Technology. 2010;**70**:272-283

[19] Jendli Z, Walrick J-C, Bocquet M, Fitoussi J. Strain rate effects on the mechanical behavior of carbon-thermoplastic matrix woven composites. In: ECCM16-16th European Conference on Composite Materials; 2014

[20] Walley S, Field J. Strain rate sensitivity of polymers in compression from low to high rates. DYMAT Journal. 1994;**1**(3):211-227

[21] Nemat-Nasser S. Introduction to high strain rate testing. In: ASM Handbook Volume 8 Mechanical Testing and Evaluation. Ohio: ASM International; 2000

[22] Qian X, Wang H, Zhang D, Wen G. High strain rate out-of-plane compression properties of aramid fabric reinforced polyamide composite. Polymer Testing. 2016;**53**:314-322

[23] Woo SC, Kim TW. High strain-rate failure in carbon/Kevlar hybrid woven composites via a novel SHPB-AE coupled test. Composites Part B: Engineering. 2016;**97**:317-328

[24] Gray GT III. Classic split-Hopkinson pressure bar testing. In: ASM Handbook Volume 8 Mechanical Testing and Evaluation. Ohio: ASM International; 2000

[25] Gray GT III, Blumenthal WR. Split-Hopkinson pressure bar testing of soft materials. In: ASM Handbook Volume 8 Mechanical Testing and Evaluation. Ohio: ASM International; 2000

[26] Chen WW, Song B. Split Hopkinson (Kolsky) Bar: Design, Testing and Applications. New York: Springer; 2011

[27] Hou JP, Ruiz C. Measurement of the properties of woven CFRP T300/914 at different strain rates. Composites Science and Technology. 2000;**60**:2829-2834

[28] Gama BA, Lopatnikov SL, Gillespie JW Jr. Hopkinson bar experimental technique: A critical review. Applied Mechanics Reviews. 2004;**57**(4):223-250

[29] Reis VL, Marini LF, Donadon MV, Dutra TA, Baldo Junior JE, Nunes de Mello WL. Experimental investigation on the influence of the geometry of carbon fiber specimen used in split Hopkinson pressure bar tests. In: 23rd ABCM International Congress of Mechanical Engineering; 2015

[30] Koerber H, Xavier J, Camanho PP, Essa YE, Martín de la Escalera F. High strain rate behaviour of 5-harness-satin weave fabric carbon–epoxy composite under compression and combined compression–shear loading. International Journal of Solids and Structures. 2015;**54**:172-182

[31] Jerabek M, Major Z, Lang RW. Strain determination of polymeric materials using digital image correlation. Polymer Testing. 2010;**29**:407-416

[32] Soutis C. Introduction: Engineering requirements for aerospace composite materials. In: Irving PE, Soutis C, editors. Polymer Composites in the Aerospace Industry. Cambridge: Elsevier Ltd; 2015. pp. 1-18

[33] Vodicka R. Thermoplastics for Airframe Applications. A Review of the Properties and Repair Methods for

Thermoplastic Composites. Melbourne, Australia: Aeronautical and Maritime Research Laboratory; 1996

[34] TenCate. TenCate Cetex and CFRT Thermoplastic Advanced Composites. Brochure. 2016. [Online]. Available: http://www.tencate.com/advancedcomposites/products/thermoplastic/default.aspx

[35] Leeser D. Thermoplastic Composites, A Proven Composite Material Technology Generates New Interest. Article. 2010. [Online]. Available: http://www.tencate.com/advancedcomposites/products/thermoplastic/default.aspx

[36] Red C. The Outlook for Thermoplastics in Aerospace Composites, 2014-2023: CompositesWorld. Article. 2014. [Online]. Available: http://www.compositesworld.com/articles/the-outlook-for-thermoplastics-in-aerospace-composites-2014-2023 [Accessed: July 25, 2017]

[37] ACP Composites. Woven Fabric Style Guide | ACP Composites. 2017. [Online]. Available: https://store.acpsales.com/products/3495/woven-fabric-style-guide [Accessed: August 8, 2017]

[38] Mallick PK. Fiber-Reinforced Composites Materials, Manufacturing and Design, Third Editon. Boca Raton: CRC Press Taylor & Francis Group; 2007

[39] Silva LFM, Reis VL, Donadon MV, Marques VEC, da Silva VQ , Corat EJ. The strain rate effects on the compressive behavior of composites. In: 22nd International Congress of Mechanical Engineering–Cobem; 2013

[40] Greenhalgh ES. Failure Analysis and Fracture of Polymer Composites. Vol. 53(9). Boca Raton: CRC Press LLC; 2009

[41] Nemat-Nasser S, Isaacs JB, Starrett JE. Hopkinson techniques for dynamic recovery experiments. Proceedings of the Royal Society of Edinburgh. Section A. Mathematical and Physical Sciences. 1991;**435**(1894):371-391

[42] Field JE, Walley SM, Proud WG, Goldrein HT, Siviour CR. Review of experimental techniques for high rate deformation and shock studies. International Journal of Impact Engineering. 2004;**30**(7):725-775

[43] Reeve S. Introduction to engineering mechanics, analysis, and design. In: ASM Handbook. Volume 21. Composites. Ohio, EU: ASM International; 2001

[44] Opelt CV. Estudo dos Modos de Falha em Compressao Uniaxial de Compósitos Avancados: Nova Proposta de Classificacao. São Paulo, Brazil: Instituo Tecnológico de Aeronáutica; 2017

[45] Cândido GM, Rezende MC, Donadon MV, De Almeida SFM. Fractografia de compósito estrutural aeronáutico submetido à caracterização de tenacidade à fratura interlaminar em modo I. Polímeros. 2012;**22**(1):41-53

[46] Cândido GM, Rezende MC, Donadon MV, Müller de Almeida SF. Fractografia de comósito estrutural aeronáutico submetido ao ensaio de tenacidade á fratura interlaminar em modo II. Polímeros. 2013;**24**:18

[47] Brent Strong A. High Performance and Engineering Thermoplastic Composites. Pennsylvania: Technomic Publishing Co., Inc; 1993

[48] Johnston NJ, Towell TW, Hergenrother PM. Physical and mechanical properties of high-performance thermoplastic and their composites. In: Carlsson LA, editor. Composite Materials Series, 7

Thermoplastic Composite Materials. New York: Elsevier Science Publishers B.V; 1991. pp. 27-71

[49] Davies P, Plummer CJG. Structure and mechanical properties of other advanced thermoplastic matrices and their composites. In: Kausch HH, editor. Advanced Thermoplastic Composites: Characterization Processing. Munich: Hanser Publishers; 1993. pp. 141-169

[50] dos Santos MN et al. Nanocomposite of photocurable epoxy-acrylate resin and carbon nanotubes: Dynamic-mechanical, thermal and tribological properties. Materials Research. 2013;**16**(2):367-374

[51] Bertholdi J, Opelt CV, Milan JCG, Coelho LAF, Lepienski CM. Propriedades mecânicas, tribológicas e térmicas de nanocompósitos de PLLA com nanotubos de carbono de paredes múltiplas. Polímeros. 2014;**24**(4):514-520

[52] Mouhmid B, Imad A, Benseddiq N, Benmedakhène S, Maazouz A. A study of the mechanical behaviour of a glass fibre reinforced polyamide 6,6: Experimental investigation. Polymer Testing. 2006;**25**:544-552

[53] Abdul Rasheed MI, Rietman B, Visser HA, Akkerman R. Experimental characterisation of recycled (glass/TUP woven fabric) flake reinforced thermoplastic composites. In: The 19th International Conference on Composite Materials; 2017. pp. 3999-4010